TEXAS A&M UNIVERSITY
J. MIKE WALKER' 66 DEPARTMENT OF MECHANICAL ENGINEERING
TURBOMACHINERY LABORATORY
TRIBOLOGY GROUP

A COMPUTATIONAL MODEL FOR THE FORCED PERFORMANCE ANALYSIS OF SELF-EQUALIZING TILTING PAD THRUST BEARINGS

Research Progress Report to the TAMU Turbomachinery Research Consortium

TRC-B&C-01-19

By

Rasool Koosha
Graduate Research Assistant

Luis San Andrés
Mast-Childs Chair Professor
Principal Investigator

TEES Project # 28-258124-00022

May 2019

EXECUTIVE SUMMARY

A self-equalizing tilting pad thrust bearing (TPTB) adjusts its pads to account for thrust collar misalignment. Work in 2019 integrates a model for the pads' leveling mechanism into the earlier thermo-elasto-hydrodynamic (TEHD) analysis tool to deliver static and dynamic load performance predictions for self-equaling TPTBs. The analysis offers an option to implement the leveling plates geometry model from a commercial solid modeling software. The model performs analysis using the exact geometry of the leveling plates and eliminates geometric simplification. The analysis, however, only accounts for the circumferential tilting of the leveling plates (around the radial axis), and assumes the contact between the leveling plates extends over their entire radial length, i.e., a line contact.

A static load analysis further determines the forces acting at the contact points of the leveling plates as well as the moments acting on them as a function of the applied load on the bearing pads. Since thrust collar misalignment rearranges the load among the pads to generate a moment on the lower leveling plates, the analysis finds tilt angles for the leveling plates to balance of moments on them. A simple Coulomb friction model further estimates the sliding friction forces acting at the contact points of the leveling plates and the rolling friction at the leveling plates pivot to be integrated into the solution. Friction forces limit the performance of the pad leveling mechanism to keep a degree of uneven loading among the pads. In addition, a Hertz contact analysis model uses the predicted forces to deliver a peak pressure for the contact area on the leveling plates.

Further, this report presents predictions from XL_ThrustBearing® for an example self-equalizing TPTB operating with a 0.01°thrust collar static misalignment. The bearing has six pads with 126 mm in OD, operates at 4krpm (maximum surface speed = 26 m/s) and a specific load/pad ranging from 0.5 to 3.5 MPa. Compared to a regular TPTB, a self-equalizing TPTB operates with up to 50% larger minimum film thickness. The peak

mechanical deformation of a regular TPTB is roughly twice that in the self-equaling TPTB. Variations of the pads peak temperature are insignificant (max of 8.6 °C) even for the regular TPTB.

NOMENCLATURE

e_c	Axial location of thrust collar center point [m].
e_p	Axial location of pivot [m].
E	Material elastic modulus [Pa].
h	Fluid film thickness [m].
h_u	Axial location of upper plates [m].
N	Shaft rotational speed [rpm], $N = \Omega\pi/30$.
P	Pressure [Pa].
R_i, R_o	Inner radius and outer radius of a pad [m].
(R_P, θ_P)	Radial and circumferential location of pivot [m],[rad.].
t_P	Pad thickness [m].
α, β	Pad tilt angles [rad.].
θ_l, θ_t	Circumferential location of leading edge and trailing edge, respectively [rad.].
φ, ψ	Thrust collar misalignment angles around X and Y axes [rad.].
μ_r, μ_s	Rolling friction coefficient, sliding friction coefficient [-].
ν	Poisson ratio [-].
Ω	Shaft angular speed [rad/s].

Vectors and Matrix

$\vec{\mathbf{d}}$	Distance from a force acting point to a selected point [m].
$\vec{\mathbf{F}}^n$	Normal force [N].
$\vec{\mathbf{F}}^f$	Friction force [N].
$\mathbf{K}_\theta$	Moment/tilt stiffness matrix [N.m/rad.].
$\vec{\mathbf{M}}$	Moment acting on leveling plates [N.m].
$\vec{\mathbf{n}}$	Surface normal vector [-].
$\vec{\mathbf{v}}$	Direction vector for the total force at a contact point [-].

Subscripts

i	Inner radius.
l	Leading edge.
lp	Lower plates.
o	Outer radius.
p	Pivot.
P	Pad.
t	Trailing edge.
up	Upper plates.

Coordinate Systems

(x, y, z)	Global Cartesian coordinate system, originate at the center of bearing housing surface.
(r, θ, z)	Global cylindrical coordinate system, originate at the center of bearing housing surface.

(γ, ξ, η) Pad local Cartesian coordinate system, originate at pivot tip and constrained to move with it.

Abbreviations

FEM	Finite Element Method.
ID	Inner diameter.
OD	Outer diameter.
TEHD	Thermo-elasto-hydrodynamic, includes pressure and thermally induced deformations.
LP	Lower leveling plates.
TPTB	Tilting Pad Thrust Bearing.
UP	Upper leveling plates.

CONTENTS

LIST OF FIGURES

1. INTRODUCTION

A self-equalizing tilting pad thrust bearing (TPTB) is an improved bearing design that, in case of thrust collar misalignment, automatically adjusts the pads' position to evenly distribute the load among the pads [1]. Figure 1 shows (a) a photograph of a self-equalizing bearing and (b) a partial schematic view of a pad leveling mechanism. A typical pad leveling system includes a series of levers called leveling plates. Bearing pads are supported on the upper plates which themselves are carried on the shoulders of two lower plates, free to move axially or to tilt (see Figure 1). The lower plates placed on the bearing housing are only free to tilt. An uneven load distribution across the pads due to collar misalignment, elastic deformations of the bearing elements, or manufacturing tolerances, induces a moment on the lower plates thus tilting them. Hence, the upper plates supporting the overloaded pads move down by pushing the other (underloaded) pads up until the moments on the lower plates are balanced.

Compared to conventional TPTBs, self-equalizing TPTBs are less expensive to install as they reduce aligning constraints and also offer a higher load capacity [2]. Due to such advantages, self-equalizing bearings have became the preferred choice in many heavy-duty applications. In particular, the American Petroleum Institute (API) requires the use of self-equalizing thrust bearings in turbines (gas and steam) and centrifugal pumps, as stated in Ref.[2].

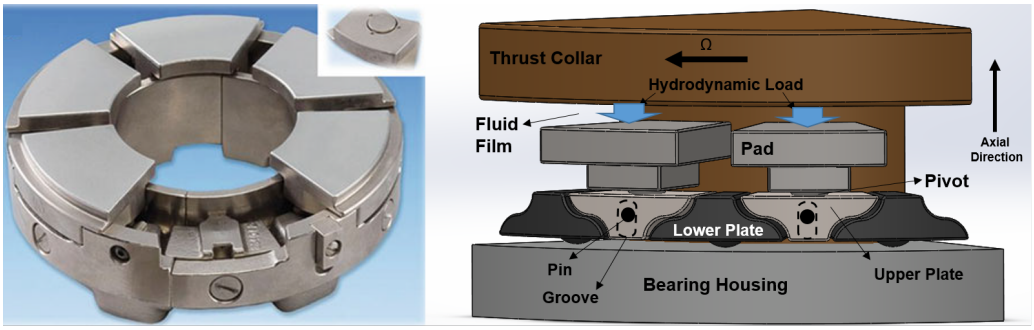

(a) (b)

Figure 1: (a): A photography of a self-equalizing TPTB (Reproduced from Ref.[3] with a permission from the publisher). A partial schematic view of a pad leveling system.

Refs. [1, 4] report uneven load distribution in thrust bearings despite the implementation of pad leveling systems. The friction forces acting at the contact points of the leveling plates reduce their aligning ability. Nonetheless, almost all predictive models assume identical load on each bearing pad and thus only conduct a single pad analysis[4–6].

The present report integrates a model for the pads' leveling mechanism into an earlier thermo-elasto-hydrodynamic (TEHD) analysis tool [7, 8] to deliver static and dynamic load performance predictions for self-equalizing thrust bearings. Section 2 scrutinizes the literature on self-equalizing fluid film thrust bearings. Section 3 describes the analysis of the pad leveling system including the static force analysis, friction model, and Hertz contact analysis. Section 4 benchmarks contact analysis from the present model versus those delivered by a commercial finite element software, i.e. ANSYS®. Section 5 uses the configuration of an example self-equalizing TPTB to demonstrate load performance predictions produced by the XL_ThrustBearing® [7, 8] software tool.

2. REVIEW OF PAST WORK

In 1987, Heshmat and Pinkus [9] theoretically study the effects of thrust collar static misalignment on the load performance of thrust bearings. The test bearings are both flat-land and taper-land fixed geometry bearings with 6, 8, and 12 number of pads. A misaligned flat-land TB could undergo lubricant cavitation over half of its geometry. As a consequence, the minimum film thickness decreases but the oil temperature rise increases to lower the bearing drag power loss. There is an increase, however, in the peak pressure and side leakage as the thrust collar misalignment increases. A taper-land thrust bearing does not experience lubricant cavitation due to color misalignment; though both the peak pressure and peak temperature rise increase substantially.

In 2001, Glavatskih and Fillon [10] extend an earlier thermo-hydrodynamic (THD) model [11] to account for both pressure and temperature induced elastic deformations of pads in a self-equalizing TPTB. The authors compare predictions obtained with and without accounting for pad elastic deformations against test data for a six-pad bearing with 228 mm in OD operating under a specific load[1] up to 2.0 MPa, and at rotor speeds up to 3 krpm (maximum surface speed[2] of ΩR_o=36 m/s). Predictions obtained accounting for pad elastic deformations better match the test results, up to 15% closer than THD predictions. The authors also report an uneven load distribution across the bearing pads despite the use of a pad leveling system [1].

In 2014, Wodtke et al. [4] compare measured fluid film thickness, fluid film pressure,

[1]Unit load or specific load = F_{pad}/A_{pad}, where F_{pad} [N] is the axial load on a pad and A_{pad} [m^2] is its area.

[2]The maximum surface speed of a thrust bearing = ΩR_o with Ω as the rotor speed [rad/s] and R_o as the outer radius [m].

and pad temperature for a large size 5.2 m OD sixteen-pad self-equalizing TPTB against predictions obtained from two distinct predictive tools. The laminar flow bearing operates at a rotor speed of 92 rpm (ΩR_o=24.5 m/s) and under an applied load of 27.7 MN, i.e. specific load = 2.6 MPa per pad. The first predictive tool is a 3D TEHD analysis developed by Souchet [12] which imposes a thermal boundary condition at the pad free surfaces using an empirical heat transfer coefficient. Using Souchet analysis, the entire fluid surrounding a pad is represented by a uniform temperature. The second tool is a fluid-structure interface (FSI) TEHD analysis developed by Pajkaczkowski [13] that couples a finite element model (FEM) of the bearing elements with a CFD model of the fluid (in the film and around the pads). Both predictive tools conduct a single pad analysis, i.e. equal loads on all pads.

Predictions from Souchet analysis [12] closely match the measured film thickness while predictions from fluid-structure interaction (FSI) analysis [13] show a substantial discrepancy. Predicted film pressure from the FSI analysis, however, better matches the test results, up to 10% closer than that delivered by Souchet's analysis. Nonetheless, pad subsurface temperature predictions from both analysis tools differ substantially from the measurements. In particular, predictions delivered by Souchet's analysis show up to a 70% difference with measured pad temperature. Despite the use of an equalizing mechanism, the authors report an uneven load distribution among the bearing pads.

In 2017, Bavassono et al. [14] improve the load capacity of a self-equalizing TPTB used in a high power-density gas turbine application. A preliminary investigation reveals uneven loads across the bearing pads despite the use of an equalizing system. The measured mean pressure on some pads are roughly twice that on other pads. The authors develop a simple analytical model for the maximum aligning capability of the equalizing system as a function of the number of pads in the bearing and the physical limit on the leveling plates' tilting. The analytical model predicts that reducing the number of pads from 10 to 8 improves the pad leveling system performance. Accordingly, Bavassono et al. implement the following changes to improve bearing load performance. Both the radial and arc lengths of the pads are increased to reduce the number of the pads and also to maximize the bearing surface area. The babbitt layer is replaced by an Aluminum-Tin (Al-Sn) based material to achieve a higher pressure and temperature durability. The pad backing portion is made of Copper-Chromium (Cu-Cr) material, instead of the original steel material, to improve heat conduction through pads. The authors state that the new design load capacity is 1.45 times that of the original bearing.

The scant literature reveals that thrust collar misalignment significantly affects the load

performance of thrust bearings. Incidentally, measurements on self-equalizing TPTBs have reported uneven load distribution across the bearing pads [1, 4, 14].

3. ANALYSIS

A self-equalizing TPTB includes a series of leveling plates. The lower plates (LP) carry the upper plates (UP) and upper plates support the bearing pads and which tilt and relocate to evenly distribute the load across the pads. Figure 2 depicts the geometry of a self-equalizing TPTB and definition of variables. The bearing pads pivot atop the upper plates; hence the pad fluid film thickness $h_{(r,\theta,t)}$ alters as the upper plates relocate along the axial direction (h_u). The upper plates are themselves carried on the shoulders of the lower plates.

At any point on a pad surface, the film thickness is a function of the thrust collar axial location ($e_{c(t)}$), thrust collar misalignment angles (φ, ψ), the upper plate axial location h_u, the pivot axial location ($e_{P(t)}$), and the pad tilt angles ($\alpha_{(t)}, \beta_{(t)}$). On pad i^{th} with a pivot located at (R^i_P, θ^i_P), the film thickness is,

$$\begin{aligned} h^i_{(r,\theta,t)} = {} & [e_c - (e^i_P + t_P) - h^i_u] + (\varphi\, r)\sin\theta - (\psi\, r)\cos\theta \\ & + (\alpha^i\, r)\sin(\theta^i_P - \theta) + (\beta^i\, r)\cos(\theta^i_P - \theta) - (\beta^i\, R^i_P) \end{aligned} \qquad \theta^i_l < \theta < \theta^i_t \tag{1}$$

where t_P is the pad thickness and (θ^i_l, θ^i_t) are the circumferential location of the pad leading edge and trailing edge, respectively.

Since the upper plates are carried by the lower plates (LP), their location (h_u) varies as the lower plates tilt with angles (θ_{lp}). To model the pad leveling system, one should derive a model for the upper plates location as a function of the lower plates tilt angles. Pad leveling systems are available in several designs, each with distinct leveling plates geometries. Thus, deriving a single analytical model for all designs is impractical. To build an analysis tool applicable for a variety of designs, the analysis here develops a numerical scheme that implements the leveling plates geometry (both the upper plate and lower plate) from any commercial solid modeling software and performs an iterative approach to find the upper plates axial location based on the lower plates tilt angles. Appendix A describes the numerical flow algorithm. The solution also determines a location for the contact points between the leveling plates. Note the analysis only considers circumferential tilting (θ_{lp}, see Figure 2) for the leveling plates.

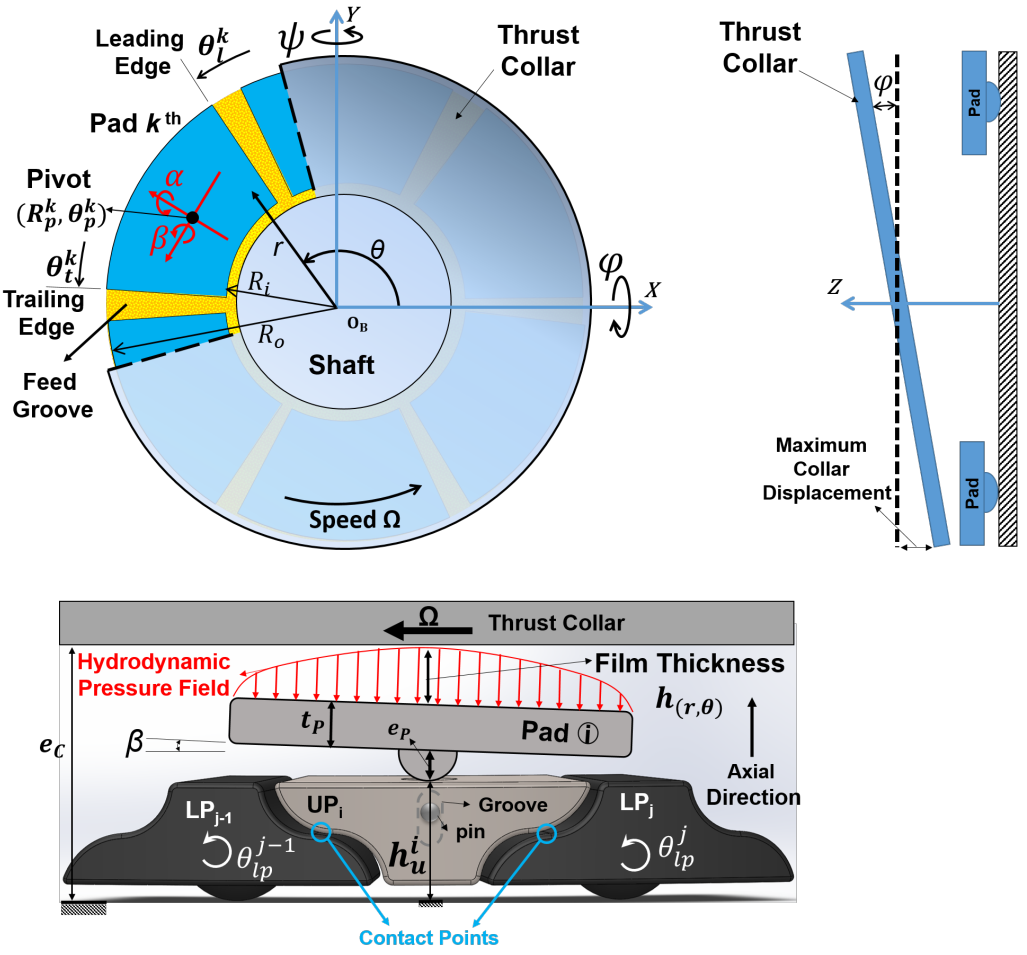

e_c Thrust collar axial location.
e_P Pivot thickness.
h Fluid film thickness.
h_u Upper plates axial location.
O_B Bearing housing center point.
(r,θ,z) Global cylindrical coordinate system.
R_p, θ_p Pivot radial and circumferential location.
R_i, R_o Pad inner and outer radius.
t_P Pad thickness.
(X,Y,Z) Cartesian coordinate system.
α, β Pad radial and circumferential tilt angles.
θ_l, θ_t Leading edge and trailing edge circumferential location.
φ, ψ Misalignment angles of thrust collar around *y* and *x* axes.
Ω Shaft rotational speed

Figure 2: Schematic view of a self-equalizing tilting pad thrust bearing. The tilting of leveling plates affects the pad fluid film thickness.

To demonstrate the numerical scheme, Figure 3 (a) shows predictions from the analysis for an example pad leveling system. The leveling plates have 50 mm in mean circumferential length. With both the lower plates held at a flat position (zero tilting), the upper

plate also positions flat with a nominal axial location of h_u = 15.601 mm. As the lower plates tilt, say to θ^1_{lp} = 8° and θ^2_{lp} = 4°, the upper plate relocates to h_u=16.196 mm. Note the leveling plates tilt angles are exaggerated here for demonstration purposes. In practice, the tilt angles of the leveling plates are very small, < 1°. Figure 3 (b) shows predictions for the upper plate axial displacement from a nominal position as a function of the lower plates tilt angles up to 1° around a flat position. Accordingly, the pad moves downward Δh_u = -0.334 mm (away from the collar to open the fluid film) with $\theta^1_{lp} = -1°$ and $\theta^2_{lp} = 1°$ and lifts Δh_u = 0.348 mm (to close the film thickness) when $\theta^1_{lp} = 1°$ and $\theta^2_{lp} = -1°$.

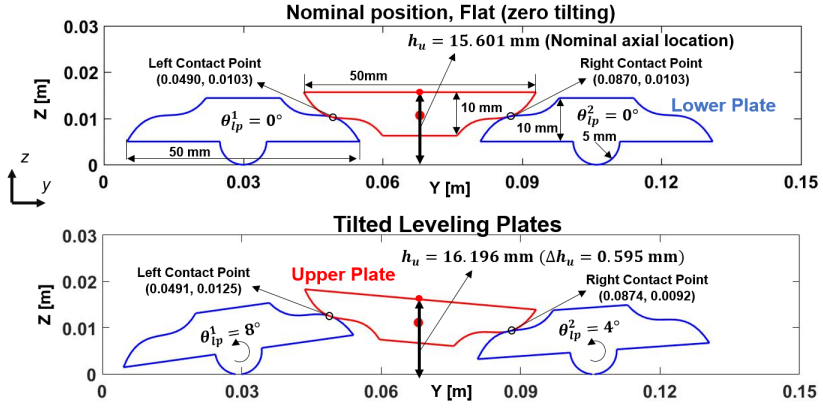

(a) Contact between Leveling Plates

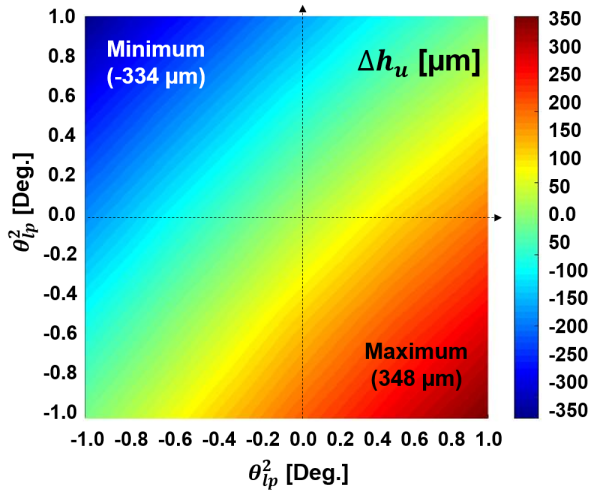

(b) Relative Displacement of Upper Plate

Figure 3: (a) Position of an upper plate with flat lower plates (with no tilting) and for tilted lower plates. (b) Predicted axial displacement of an upper plate relative to nominal height vs. lower plates tilt angles.

Static Force Analysis of a Pad Leveling System

Figure 4 shows a schematic view of an upper plate (UP) making contact with two lower plates (LP). An equivalent hydrodynamic load $\vec{\mathbf{F}}^{n}_{pad}$ (normal) and a friction force $\vec{\mathbf{F}}^{f}_{piv}$ (tangential) acts where the pad pivot seats at the top surface of the upper plate. A pin attached to the upper plates that slides inside a groove in the bearing housing (or the other way around) prevents the upper plates from displacing along the y-axis (horizontal direction). Thus, force $\vec{\mathbf{F}}_{pin}$ acts on the upper plates at the pin location.

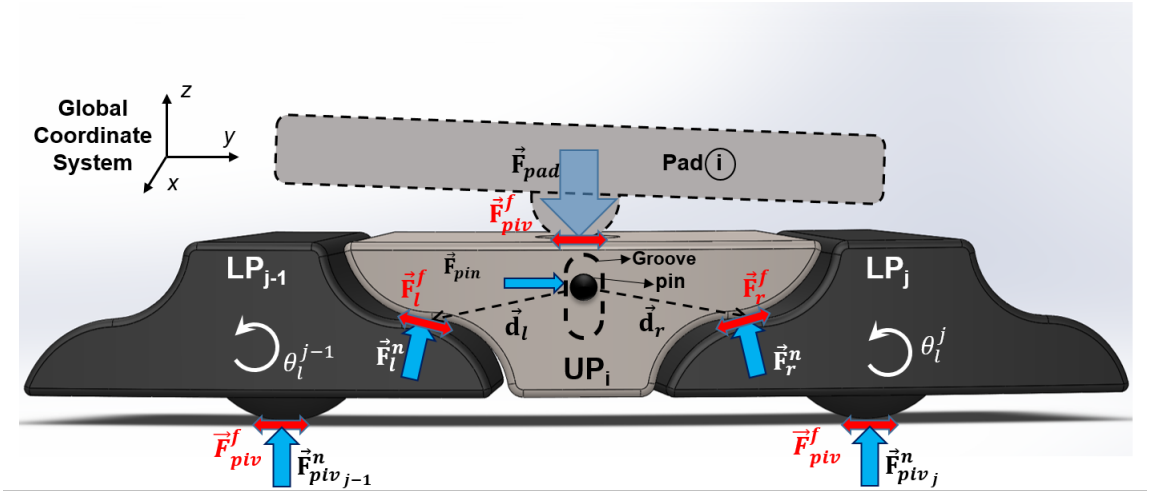

Figure 4: Schematic view of lower and upper leveling plates with the forces acting on them.

For an upper plate to be at an equilibrium state, the forces and moments acting on it should balance. Assuming the weight of the leveling plates is negligible, the equations for force and moment balance in an upper plate are

$$\sum \vec{\mathbf{F}} = \vec{\mathbf{F}}^{n}_{l} + \vec{\mathbf{F}}^{f}_{l} + \vec{\mathbf{F}}^{n}_{r} + \vec{\mathbf{F}}^{f}_{r} + \vec{\mathbf{F}}^{n}_{pin} + \vec{\mathbf{F}}^{n}_{pad} + \vec{\mathbf{F}}^{f}_{piv} = 0 \tag{2a}$$

$$\sum \vec{\mathbf{M}}_{pin} = \vec{\mathbf{d}}_{l} \times [\vec{\mathbf{F}}^{n}_{l} + \vec{\mathbf{F}}^{f}_{l}] + \vec{\mathbf{d}}_{r} \times [\vec{\mathbf{F}}^{n}_{r} + \vec{\mathbf{F}}^{f}_{r}] + \vec{\mathbf{d}}_{pad} \times [\vec{\mathbf{F}}^{n}_{pad} + \vec{\mathbf{F}}^{f}_{piv}] = 0 \tag{2b}$$

where vector $\vec{\mathbf{d}} = (d^{y}, d^{z})$ is the distance from the pin to a force acting point. $\vec{\mathbf{F}}^{n}$ is the normal force at a contact point and $\vec{\mathbf{F}}^{f}$ is the respective tangential (friction) force.

As stated in Ref.[15], a friction force at a bearing pad pivot is either a sliding friction for a ball and socket type, or a rolling friction for a rocker back type. The friction forces at the contact points between leveling plates are sliding friction as the leveling plates are assumed to remain fixed along the y-axis. The friction forces at the contact point of the

lower plates pivot and the bearing housing might be either sliding or rolling based on the type of pivot in the lower plates. For both sliding and rolling type motions, the friction force ($|F^f|$) is modeled using a friction coefficient (μ). The rolling and sliding friction forces are,

$$\text{Rolling friction} \qquad |F^f| \leq \mu_r |F^n| \tag{3a}$$

$$\text{Sliding friction} \qquad |F^f| \leq \mu_s |F^n| \tag{3b}$$

where μ_r is a rolling friction coefficient with a typical value ranging from 0.01 to 0.1 [16] and μ_s is a sliding friction coefficient ranging from 0.01 to 0.4. Both the sliding and rolling friction coefficients are functions of the materials elastic modulus and hardness, the lubricant properties, and surface condition [17]. Particular to a pad leveling system, surface condition varies over the time as the leveling plates wear.

The numerical scheme described in Appendix A delivers a location for the contact points between the leveling plates as well as the contact surface normal ($\vec{\mathbf{n}}$) and tangential ($\vec{\mathbf{t}}$) vectors. Hence, at a contact point, the total force (equals the sum of normal and friction forces) is,

$$\vec{\mathbf{F}} = \vec{\mathbf{F}}^n + \vec{\mathbf{F}}^f = |F^n|\vec{\mathbf{n}} + \mu|F^n|\vec{\mathbf{t}} = |F^n|\left(\vec{\mathbf{n}} + \mu\,\vec{\mathbf{t}}\right) = |F^n|\sqrt{1+\mu^2}\begin{Bmatrix} v_l^y \\ v_l^z \end{Bmatrix} = |F|\vec{\mathbf{v}} \tag{4}$$

where $|F|$ and $\vec{\mathbf{v}}$ represent the magnitude and direction vector for the resultant force, respectively. Eqns. (2) and (4) are solved to calculate a magnitude for the contact forces acting on the left side ($|F_l|$) and right side ($|F_r|$) of the upper plate,

$$|F_l| = \frac{v_{pad}^z(d_r^y v_r^z - d_r^z v_r^y) - v_r^z(d_{pad}^y v_{pad}^z - d_{pad}^z v_{pad}^y)}{v_l^z(d_r^y v_r^z - d_r^z v_r^y) - v_r^z(d_l^y v_l^z - d_l^z v_l^y)}|F_{pad}| \tag{5a}$$

$$|F_r| = \frac{v_l^z(d_{pad}^y v_{pad}^z - d_{pad}^z v_{pad}^y) - v_{pad}^z(d_l^y v_l^z - d_l^z v_l^y)}{v_l^z(d_r^y v_r^z - d_r^z v_r^y) - v_r^z(d_l^y v_l^z - d_l^z v_l^y)}|F_{pad}| \tag{5b}$$

where F_{pad} is the hydrodynamic force acting on a pad top surface.

Figure 5 shows a schematic view of a lower plate carrying two upper plates on its shoulders. The friction forces at the contact points of the leveling plates are of sliding type whereas the friction force at the pivot is of rolling type. Hence, the moment acting on the

lower plate is,

$$\vec{M}_{piv} = \vec{\mathbf{d}}_l \times \vec{\mathbf{F}}_l + \vec{\mathbf{d}}_r \times \vec{\mathbf{F}}_r + \vec{\mathbf{d}}_{piv} \times \vec{\mathbf{F}}_{piv} \rightarrow 0 \tag{6}$$

where, $\vec{\mathbf{d}}$ is a distance from the lower plate mass center to the respective contact point. Note the forces $\vec{\mathbf{F}}_r$ and $\vec{\mathbf{F}}_l$ represent an equivalent force at the contact points, each equal to the sum of the normal force and friction forces

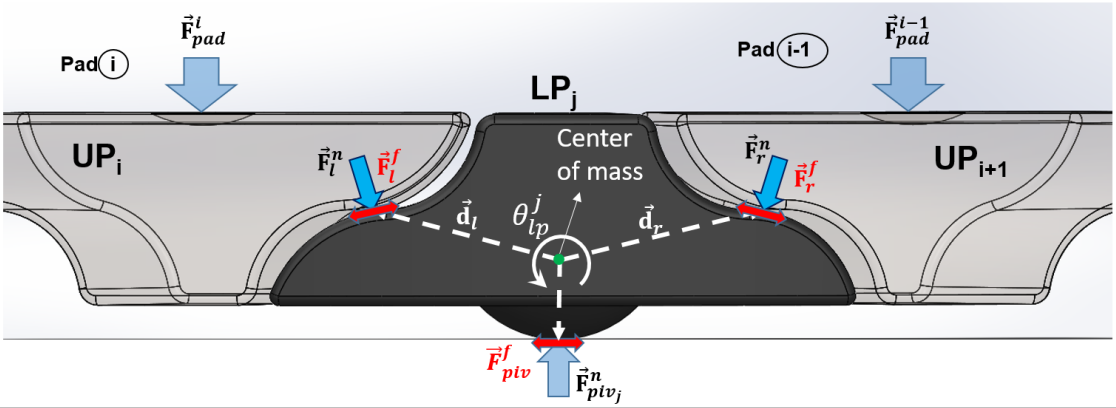

Figure 5: Schematic view of forces acting on lower and upper plates.

Once the moments acting on the lower plates are derived, the next step is to perform a Newton-Raphson technique to obtain the lower plates tilt angles (θ_{lp}) that satisfy the balance of moments on them. Expanding the moment expression using the linear terms in the Taylor series about a point $(\theta_{l_0}^1, \ldots, \theta_{l_0}^{N_{Pad}})$ gives,

$$\vec{M}_{piv}^i\Big|_{(\theta_l^1,\ldots,\theta_l^{N_{Pad}})} = \vec{M}_{piv}^i\Big|_{(\theta_{l_0}^1,\ldots,\theta_{l_0}^{N_{Pad}})} + \sum_{j=1}^{N_{Pad}} K_{\Theta_{ij}}(\theta_l^j - \theta_{l_0}^j) \tag{7}$$

where $K_{\Theta_{ij}}$ is a moment/tilt stiffness coefficient, i.e,

$$K_{\Theta_{ij}} = \frac{\partial \vec{M}_{piv}^i}{\partial \theta_l^j}\Big|_{(\theta_l^1,\ldots,\theta_l^{N_{Pad}})} \tag{8}$$

Note the number of both lower plates and upper plates in a self-equalizing TPTB equals to the number of pads (N_{Pad}). Then, the lower plates tilt angles at each iteration of the Newton-Raphson technique are,

$$\{\theta\} = \{\theta_0\} + [\mathbf{K}_\theta]^{-1}\{M_{piv}\} \tag{9}$$

$$\begin{Bmatrix} \theta_{lp}^1 \\ \theta_{lp}^2 \\ \theta_{lp}^3 \\ \vdots \\ \theta_{lp}^{N_{Pad}} \end{Bmatrix} = \begin{Bmatrix} \theta_{lp_0}^1 \\ \theta_{lp_0}^2 \\ \theta_{lp_0}^3 \\ \vdots \\ \theta_{lp_0}^{N_{Pad}} \end{Bmatrix} - \begin{bmatrix} \frac{\partial \vec{M}_{piv}^1}{\partial \theta_l^1} & \frac{\partial \vec{M}_{piv}^1}{\partial \theta_l^2} & \frac{\partial \vec{M}_{piv}^1}{\partial \theta_l^3} & \cdots & \frac{\partial \vec{M}_{piv}^1}{\partial \theta_l^{N_{Pad}}} \\ \frac{\partial \vec{M}_{piv}^2}{\partial \theta_l^1} & \frac{\partial \vec{M}_{piv}^2}{\partial \theta_l^2} & \frac{\partial \vec{M}_{piv}^2}{\partial \theta_l^3} & \cdots & \frac{\partial \vec{M}_{piv}^2}{\partial \theta_l^{N_{Pad}}} \\ \frac{\partial \vec{M}_{piv}^3}{\partial \theta_l^1} & \frac{\partial \vec{M}_{piv}^3}{\partial \theta_l^2} & \frac{\partial \vec{M}_{piv}^3}{\partial \theta_l^3} & \cdots & \frac{\partial \vec{M}_{piv}^3}{\partial \theta_l^{N_{Pad}}} \\ \vdots & \vdots & \vdots & \ddots & \vdots \\ \frac{\partial \vec{M}_{piv}^{N_{Pad}}}{\partial \theta_l^1} & \frac{\partial \vec{M}_{piv}^{N_{Pad}}}{\partial \theta_l^2} & \frac{\partial \vec{M}_{piv}^{N_{Pad}}}{\partial \theta_l^3} & \cdots & \frac{\partial \vec{M}_{piv}^{N_{Pad}}}{\partial \theta_l^{N_{Pad}}} \end{bmatrix}^{-1} \begin{Bmatrix} \vec{M}_{piv}^1 \\ \vec{M}_{piv}^2 \\ \vec{M}_{piv}^3 \\ \vdots \\ \vec{M}_{piv}^{N_{Pad}} \end{Bmatrix} \tag{10}$$

A first degree forward finite difference method evaluates the derivatives in Eqn. (9) as,

$$\frac{\partial \vec{M}_{piv}^i}{\partial \theta_{lp}^j} = \frac{\vec{M}_{piv}^i\Big|_{(\theta_{lp}^1,\ldots,\theta_{lp}^j+\Delta\theta_{lp}^j,\ldots,\theta_{lp}^{N_{Pad}})} - \vec{M}_{piv}^i\Big|_{(\theta_{lp}^1,\ldots,\theta_{lp}^j,\ldots,\theta_{lp}^{N_{Pad}})}}{\Delta\theta_{lp}^j} \tag{11}$$

Hertz Contact Analysis for the Leveling Plates

The analysis in the prior section, see Eqn.(5), calculates a magnitude for the forces acting on the contact points of the leveling plates. This section describes a Hertz contact analysis model using the contact forces to predict a peak pressure over the contact area. The contact between the leveling plates is modeled as a cylinder-on-cylinder solid contact (line). Note the wear rate at the contact area of the leveling plates is directly proportional to the contact pressure. Hence, a proper leveling plates design should minimize the peak pressure at the contact points.

The analysis adopts well-known formulas stated by Shigley [18]. Let E and ν be the elastic modulus and the Poison ratio for the leveling plates material, respectively, the peak pressure over the leveling plates contact area as [18],

$$P_{max} = \frac{2F}{\pi b L} \tag{12}$$

where

$$b = \sqrt{\frac{8F\frac{1-\nu^2}{E}}{\pi L\left(\frac{1}{R_1}+\frac{1}{R_2}\right)}} = \sqrt{\frac{8\frac{1-\nu^2}{E}}{\pi L\left(\frac{1}{R_1}+\frac{1}{R_2}\right)}}\sqrt{F} \tag{13}$$

with b as half of the half-width of the contact area, L as the length of the contact, and F is the contact force. R_1 and R_2 are the surface radii curvature at the line of contact as Figure 6 shows.

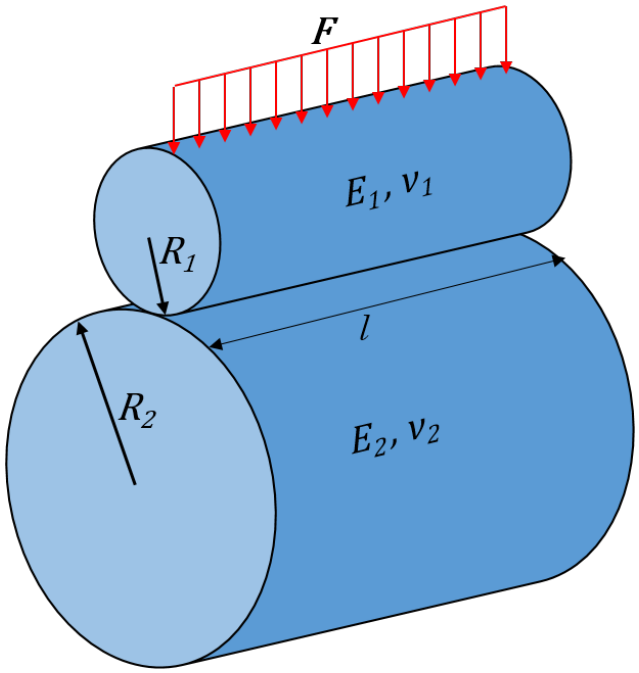

Figure 6: Schematic view of contact between two cylinders.

Note the fluid film thickness equation implemented in the analysis does not yet account for the leveling plates deformations. In addition, the leveling plates structural stiffness is not included in the calculation of the bearing force coefficients.

4. VALIDATION OF CONTACT ANALYSIS

To evaluate the present contact analysis, this report models an example pad leveling system in a commercial finite element software tool, i.e ANSYS® structural analysis, to perform contact analysis and to benchmark the results versus predictions delivered by the XL_ThrustBearing® tool. The pad leveling system includes lower plates (LP) and upper plates (UP) assembled on the bearing housing. Figure 1 shows the leveling plates modeled in the commercial software in both an exploded mode and an assembled mode.

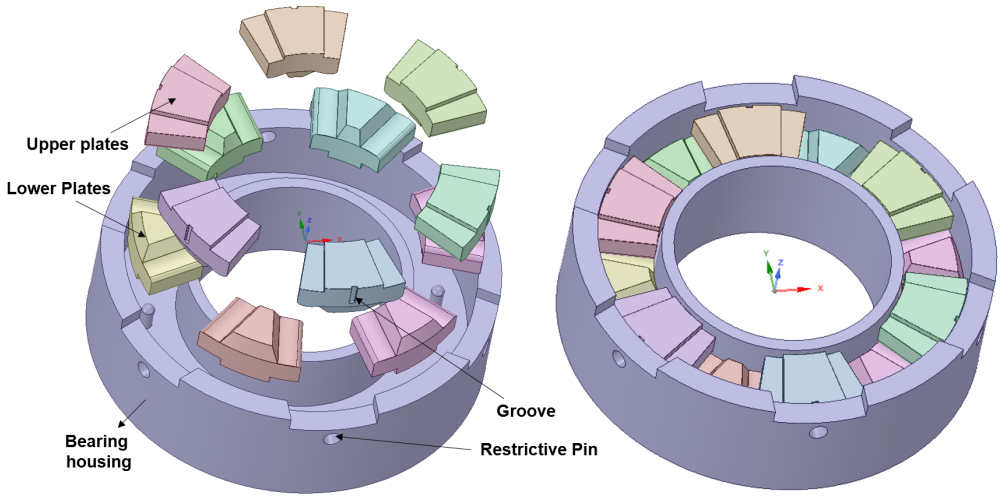

(a) Exploded View Mode (b) Assembled View Mode

Figure 7: A pad leveling system modeled in a commercial finite element software to perform contact analysis.

The pad leveling system modeled here is a part of a test self-equalizing tilting pad thrust bearing with 126.8 mm in OD and 63.4 mm in ID. The bearing operating condition determines the load applied on each pad and which is transfered to the upper plates through the pad pivots. Figure 8 shows leveling plates meshed by the commercial software with boundary conditions imposed on them to perform the contact analysis. The equivalent hydrodynamic load is applied on the mean radial length of the upper plate top surface exactly where the pad pivot seats. The groove on the upper plate outer radius is set to zero displacement along the radial and circumferential directions to simulate the restrictive pin in the actual design. A frictional contact between the leveling plates implements a friction coefficient of $\mu = 0.2$, based on the measured contact frictions reported[3] in [19].

[3]Ref. [19] states that for temperature < 200°C, the measured sliding friction coefficients for several sample materials including steel-on-steel and cooper-on-cooper are roughly same, $\mu_s \approx 0.2$.

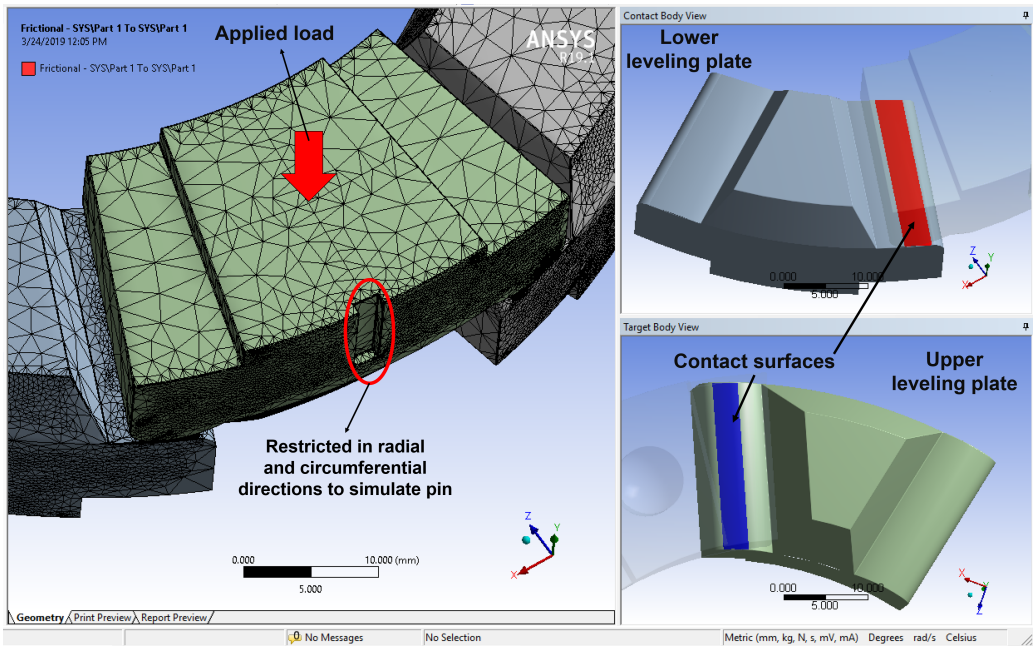

Figure 8: Boundary conditions applied on leveling plates and the arrangement of contact surfaces to perform analysis in a commercial software.

Figure 9 through 11 portray contact analysis from the commercial software for the example equalizing system under an applied load on the upper plates ranging from 664 N to 4650 N. The range of applied load relates to the thrust bearing operating under a light load of 0.5 MPa to a heavy load of 3.5 MPa specific load per pad. The outputs of the analysis are a contact status map and the pressure profile over the contact area. In Figure 9, operating under a light load of 664 N load per pad, the peak pressure at the contact points of the leveling plates ranges to from 314 MPa to 372 MPa over the contact line except for near the edges where stress concentration occurs and the peak pressure rises up to 490 MPa. The status of the contact region shows the upper plate slides over the surface of the lower plate. In Figure 11 with the load increasing to 4650 N, the peak pressure ranges from 745 MPa to 890 MPa over the center of the contact line and to 1780 MPa at the edges of the line contact.

Figure 12 compares the peak contact pressures delivered by the commercial FE analysis software against those produced by the Hertz contact analysis implemented in the XL_ThrustBearing® tool versus pad specific load ranging from 0.5 MPa to 3.5 MPa. The friction coefficient for the FE analysis is $\mu = 0.2$. The predicted Hertz contact analysis falls within the predicted range delivered by the commercial software. Note the results in Figure 12 do not include the stress concentration at both ends of the contact line.

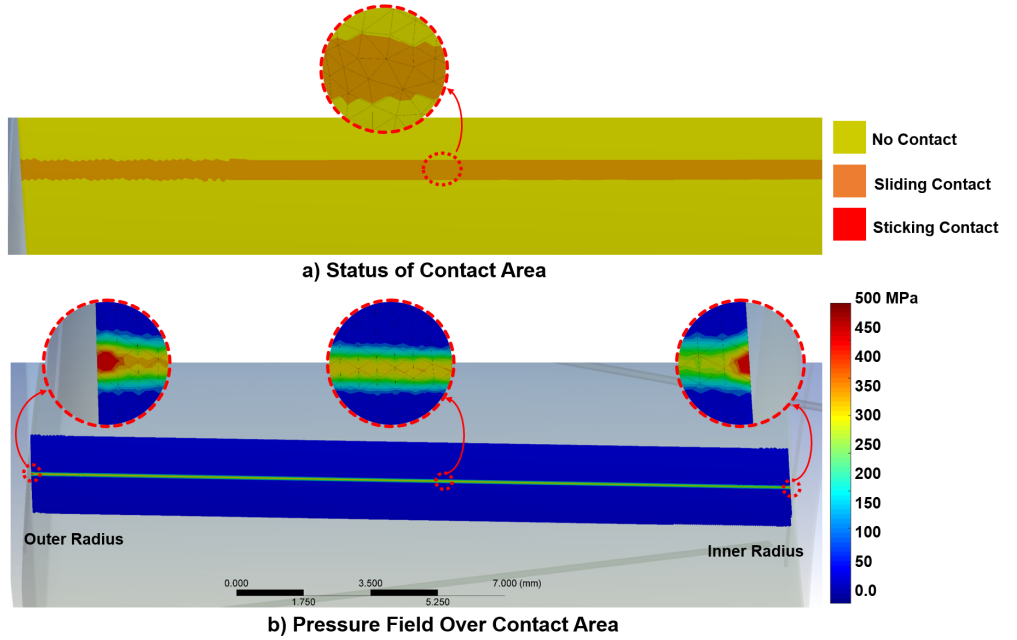

Figure 9: Contact analysis on leveling plates under 664 N load equivalent to a light load of 0.5 MPa specific pressure per pad. Friction coefficient μ=0.2.

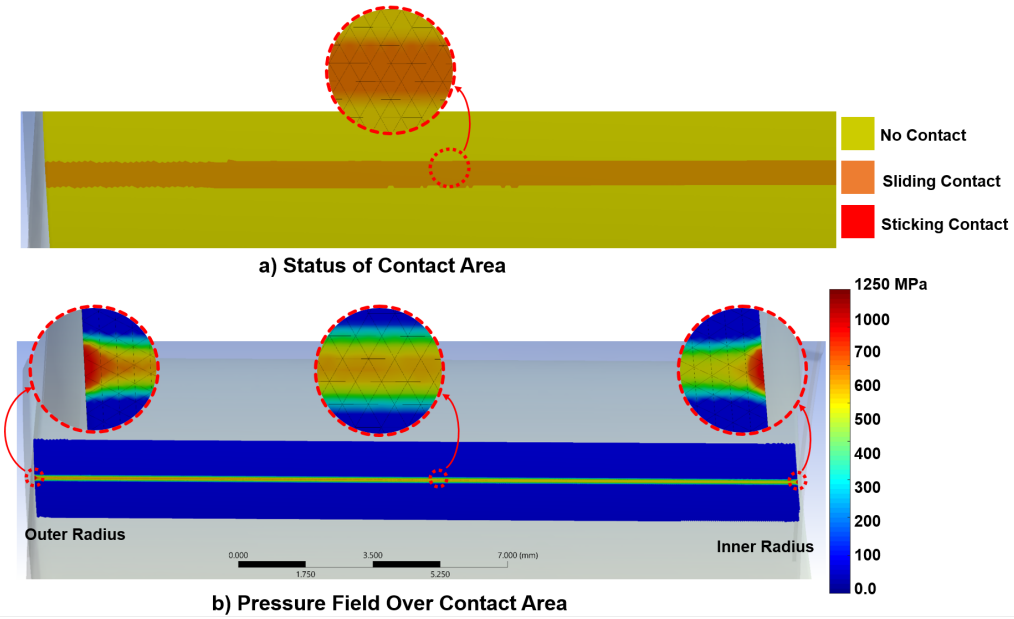

Figure 10: Contact analysis on leveling plates under 2630 N load equivalent to a medium load of 2.0 MPa specific pressure per pad. Friction coefficient μ=0.2.

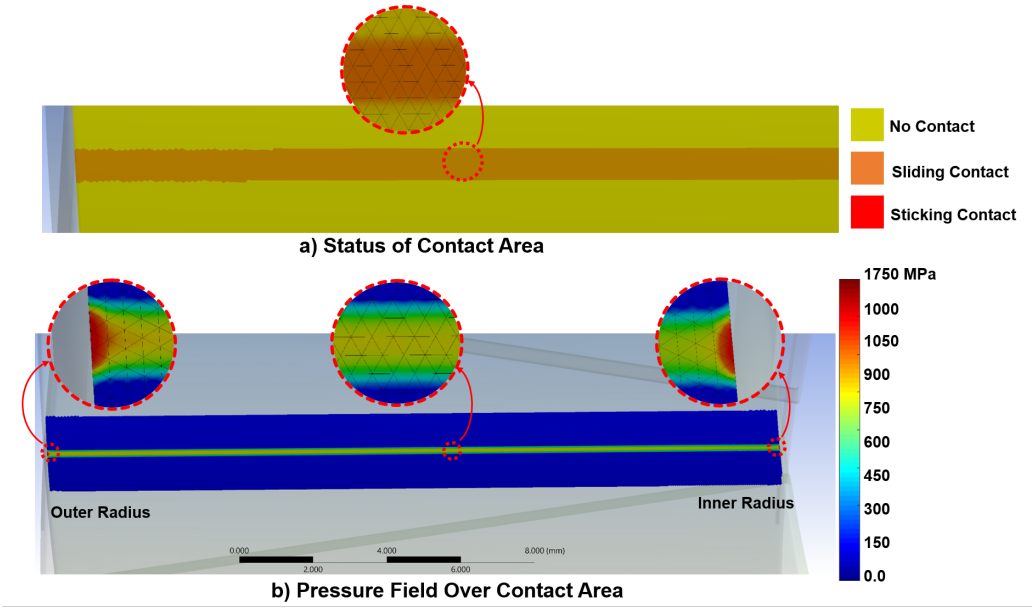

Figure 11: Contact analysis on leveling plates under 4560 N load equivalent to a heavy load of 3.5 MPa specific pressure per pad. Friction coefficient μ=0.2.

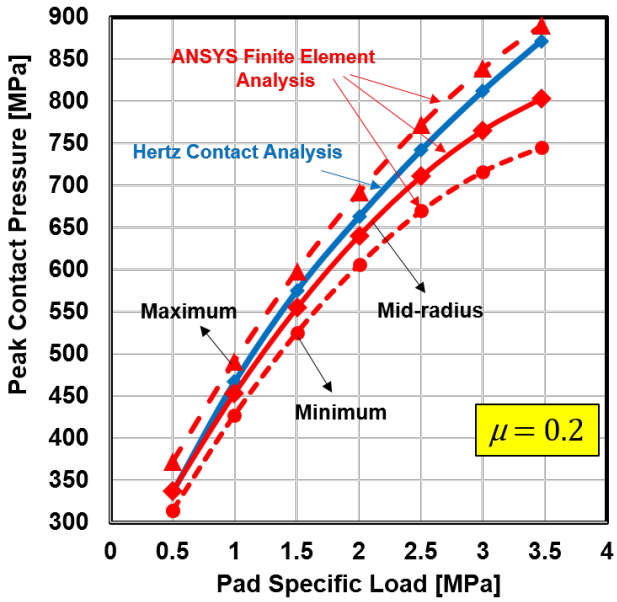

Figure 12: Comparison of contact peak pressure on leveling plates vs pad specific load predicted by a commercial software finite element analysis and by a Hertz contact analysis. Friction coefficient μ=0.2.

5. Further Predictions for an Example Self-Equalizing Tilting Pad Thrust Bearing

This section describes thermo-elasto-hydrodynamic (TEHD) predictions from the current model for an example self-equalizing tilting pad thrust bearing[4] (TPTB). Table 1 highlights the geometry, lubricant properties, and operating conditions for the test bearing.

Table 1: Geometry and operating conditions for an example self-equaling TPTB used for demonstrating predictions delivered by the present model.

Bearing properties			
Number of pads, N_P		6	-
Inner diameter		63.4	mm
Outer diameter		126.8	mm
Pad arc length		50	°
Pivot circum. offset		50	%
Pivot radial offset		50	%
Pad thickness		14.5	mm
Babbitt thickness*		2	mm
Pad area, A_P		13.14	cm^2
Operating condition			
Specific load		1-3	MPa
Shaft rotational speed		4	krpm
Supply pressure*		0	bar
Fluid properties		ISO VG32	
Viscosity-temperature coefficient, α^*_{TV}		0.0247	1/°C
Viscosity, μ_{Su} (at 46°C)		22	cPoise
Density, ρ		821	kg/m^3
Specific heat capacity, c_P		2.17	kJ/(kg· °C)
Thermal conductivity, , κ		0.13	W/(m· °C)
Pad material properties	Steel	Babbitt	
Thermal conductivity, κ_P	51	55	W/(m·°C)
Elasticity modulus, E	210	52	GPa
Thermal expansion, α_T	12	24	10^{-6}/°C
Poisson ratio, ν	0.3	0.3	-
Analysis Assumptions			
Finite Element reference temperature*		20	°C
Thermal mixing coefficient.* λ_{mix}		0.4-0.6	
Heat Transfer coefficient on back of pad* η		100	W/(m^2·°C)

*Assumed or calculated based on the available data .

The test bearing has 6 pads with 126.8 mm in OD and 50°in arc length and operates at 4.0 krpm ($R_o\Omega$ =26.8 m/s) and under specific load ranging from 1 MPa to 3 MPa, i.e from a lightly loaded to an heavily loaded condition. Figure 13 depicts an schematic view of the pads and leveling plates arrangement with respect to a global coordinate system (X, Y, Z).

[4]A commercial design manufactured by Hunan Sund Industrial and Technological Co. in PRC and donated to Turbomachinery Laboratory.

See prior sections for geometry and specifications of the pad leveling system. Mineral oil ISO VG32 is used for lubrication at a supply temperature of 46°C.

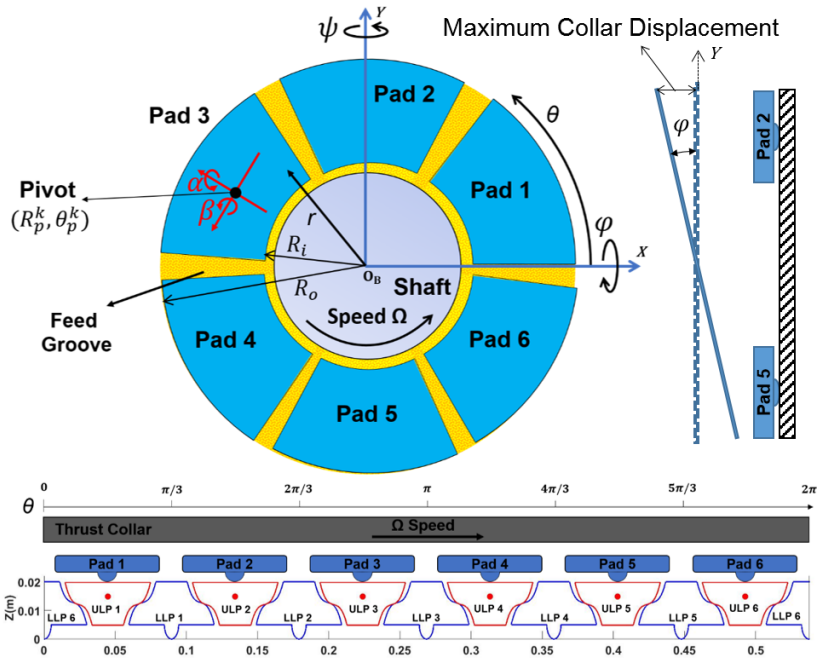

Figure 13: Schematic view of an example self-equaling TPTB

Figures 14 through 16 portray characteristic load performance predictions for the test bearing operating under a φ= 0.01° thrust collar static misalignment around the X-axis. The bearing operates at 4 krpm and under 1 MPa specific load. Note the maximum displacements of the thrust collar due to the misalignment is $R_o\varphi$= 11.25 μm and which equals to 75% of the nominal minimum film thickness if the bearing operates under the same load and without any collar misalignment. A positive thrust collar misalignment around the X-axis opens the fluid film thickness on pads ① to ③ and closes the film on pads ④ to ⑥.

Predictions follow for three cases: (a) without including the pad leveling system model to simulate the performance of a regular TPTB, (b) with the pad leveling system model included but disregarding the friction forces, i.e. an ideal performance, and (c) with the pad leveling system model included and accounting for the friction forces at the contact points, i.e. a realistic performance. The sliding friction coefficient and rolling friction coefficient used for case (c) are μ_s=0.2 and μ_r=0.01, respectively, based on measurements in Refs. [17, 19].

Figure 14 depicts the fluid film thickness field and pressure field predicted for the test TPTB under the three analysis cases. The regular TPTB shows significant variations of fluid film thickness and pressure across the pads. The fluid film on pad ② has a minimum thickness of h_{min} = 25.3μm, roughly two and half times of that on pad ⑤ (h_{min} = 9.8 μm). Variations of pressure field magnitude across the pads are, however, more substantial, such that, the peak pressure over pad ⑤ (P_{Peak} = 11.3 MPa) is eight times of that over pad ② (P_{Peak} = 1.4 MPa). In Figure 14 (b), due to the use of an ideal pad leveling system (disregarding friction forces), the fluid film thickness and pressure fields are nearly identical among the pads with a minimum film thickness of h_{min} = 15 μm and a peak pressure of P_{Peak} = 4.7 MPa. In Figure 14 (c), as the analysis accounts for friction forces, differences still remain in the film thickness and pressure fields across the pads. The remaining differences are, however, significantly reduced compared to those in the regular TPTB. The peak pressure of pads ranges from 3.6 MPa to 5.8 MPa and the minimum film thickness varies between 17.1 μm and 13.5 μm.

Figure 15 demonstrates the predicted temperature distribution in the fluid film domain on the left side and in the bearing pads on the right side. The differences of both fluid film peak temperature and pad peak temperature are not significant even for the regular TPTB. The peak temperature of the regular bearing varies only 8.6 °C, from a minimum of 70.3 °C in pad ② to a maximum of 78.9 °C in pad ⑤. Differences in the peak pad temperature vanish in case (b) for the ideal self-equalizing bearing. In case (c), the self-equalizing bearing with friction included shows a maximum differences of 5 °C in the pads peak temperature.

Figure 16 shows three graphs depicting pad elastic deformations for an operation under load/pad of 2.0 MPa per pad. The left graphs show mechanical (pressure) deformations, the middle graphs show thermal (temperature variations) deformations, and the right graphs depict deformations due to the combined action of both pressure and temperature. Observe the mechanical deformations are negative and which means the pads displace away from the thrust collar to open the film thickness. On the other hand, the thermal deformations of the pad top surface are positive and push the pad closer to the thrust collar to reduce the fluid film thickness. Pressure induced deformations show significant differences across the bearing pads and rise up to 4 μm in magnitude for the regular TPTB (case (a)) where pressure field is concentrated on pad ⑤. In case (b), disregarding the friction forces leads to nearly identical pressure deformations for all pads with a maximum of 1.6 μm. The realistic self-equalizing TPTB (case (c), one with friction) shows a peak pressure

deformation of 2.1 μm.

Pad thermal deformations follow the same trend as the pad temperature field (in Figure 15) to show marginal variations across the pad. Note that, in general, thermal deformations are larger than pad mechanical deformations and dominate the pad overall deformations shown on the right side of Figure 16.

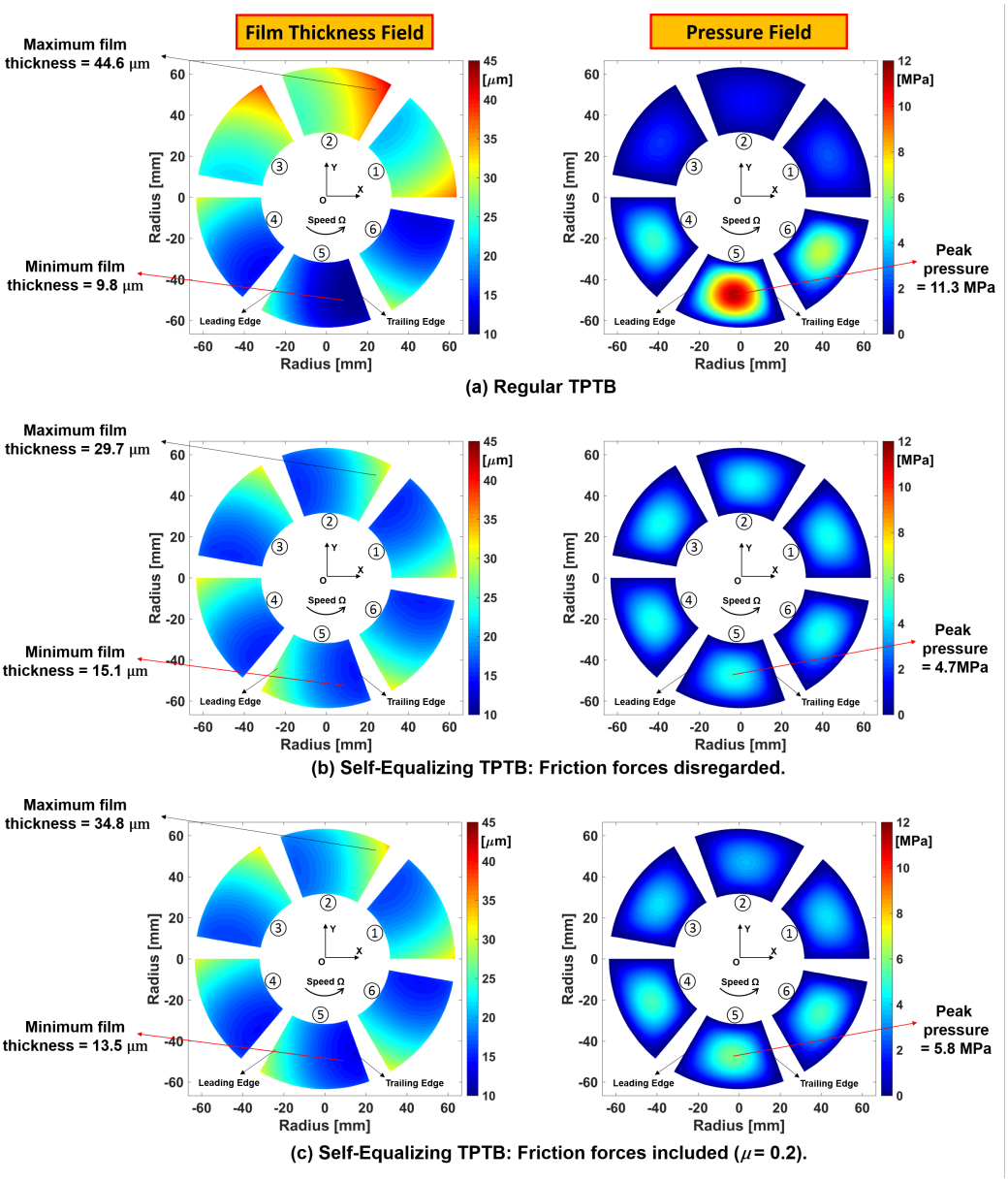

Figure 14: Predicted fluid film thickness field (left) and pressure field (right) for a TPTB of (a) regular type, (b) self-equalizing type without including contact friction forces, and (c) self-equaling type with contact friction forces included. Bearing operates with 0.01° thrust collar (static) misalignment. Rotor speed = 4krpm, specific load per pad = 2 MPa, μ= 0.2.

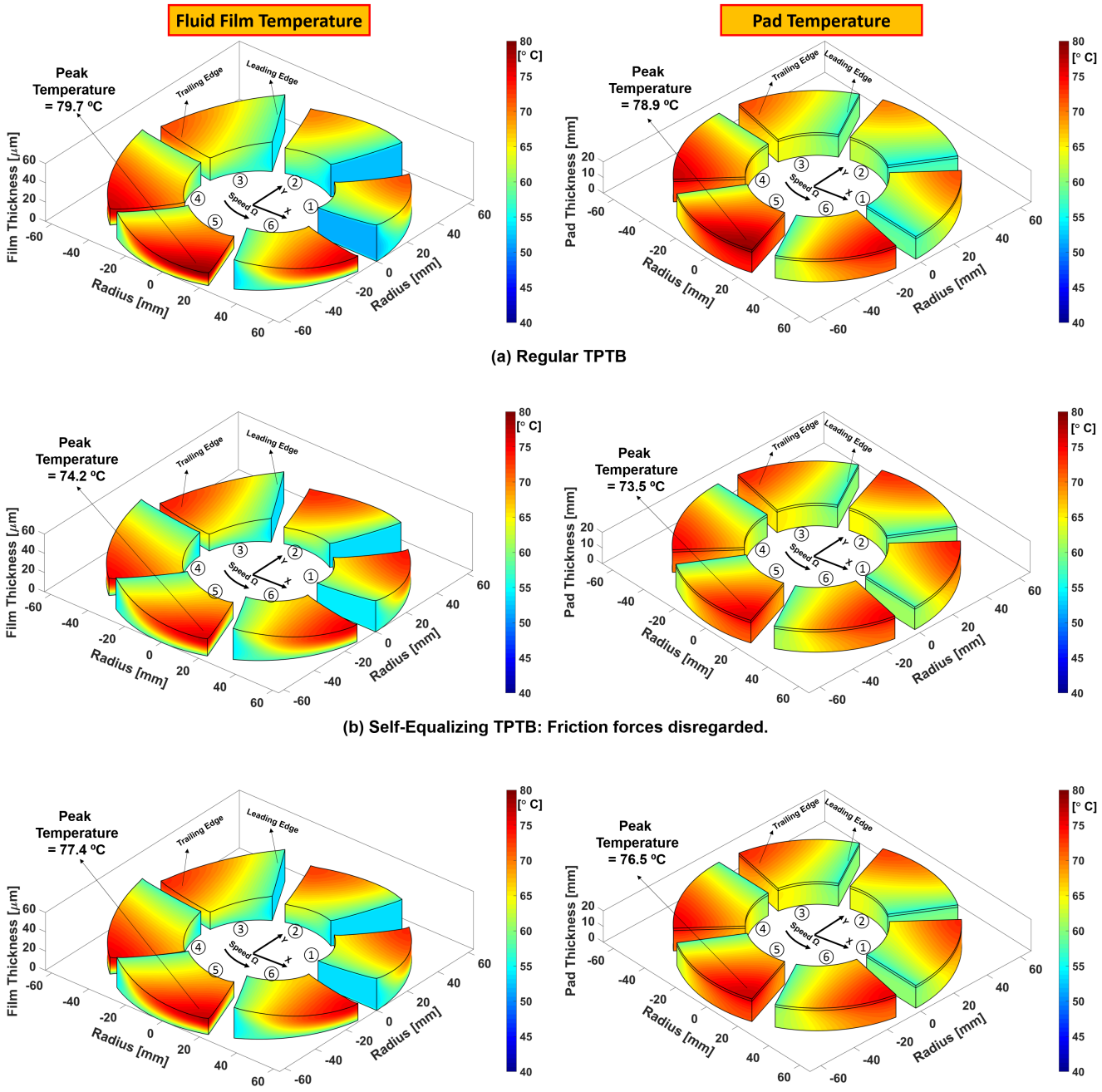

(a) Regular TPTB

(b) Self-Equalizing TPTB: Friction forces disregarded.

(c) Self-Equalizing TPTB: Friction forces included (μ= 0.2).

Figure 15: Predicted fluid film temperature field (left) and pad temperature field (right) for a TPTB of (a) regular type, (b) self-equalizing type without including contact friction forces, and (c) self-equaling type with contact friction forces included. Bearing operates with 0.01° thrust collar (static) misalignment. Rotor speed = 4krpm, specific load per pad = 2 MPa, μ= 0.2.

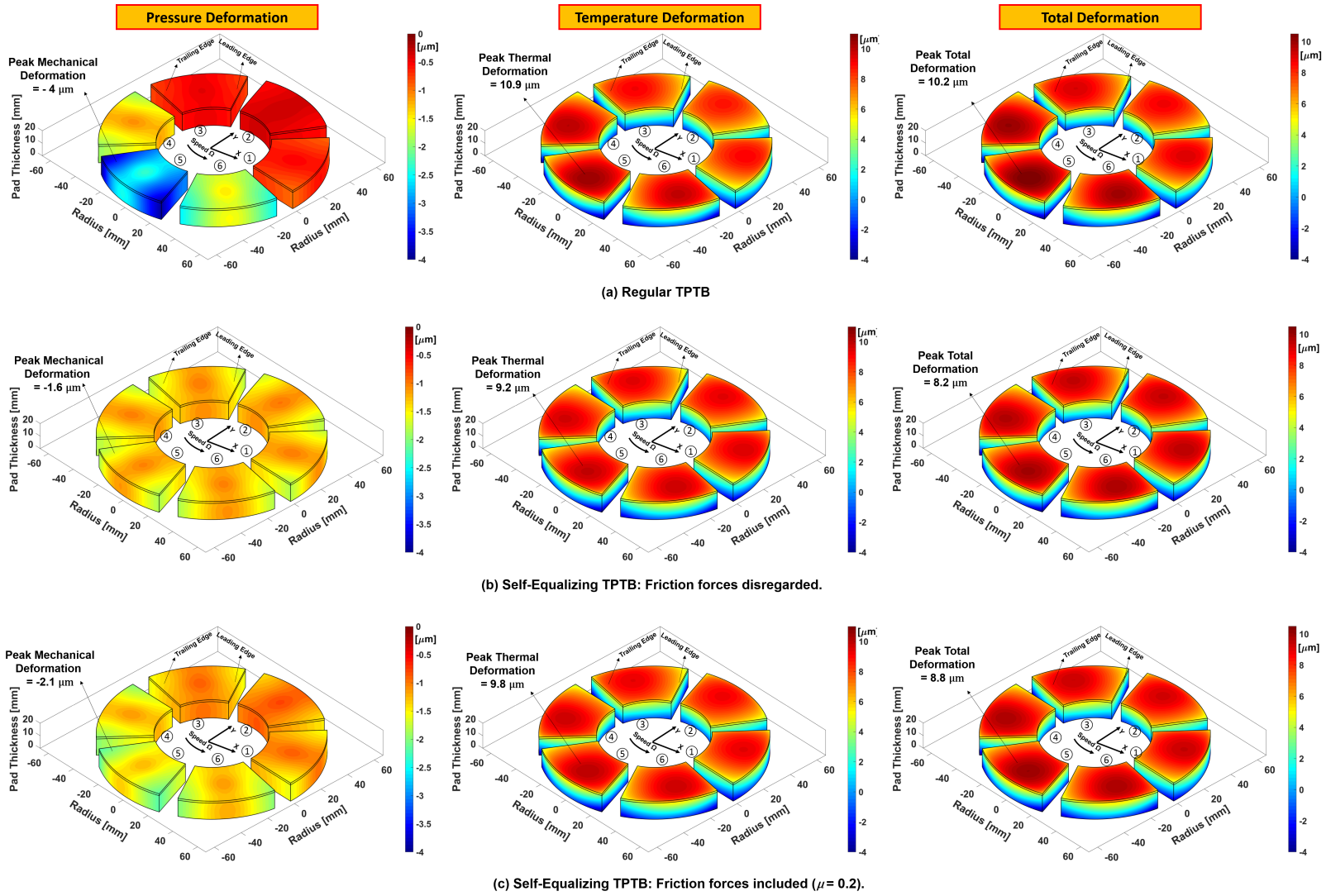

Figure 16: Predicted fluid film temperature field (left) and pad temperature field (right) for a TPTB of (a) regular type, (b) self-equalizing type without including contact friction forces, and (c) self-equaling type with contact friction forces included. Bearing operates with 0.01° thrust collar (static) misalignment. Rotor speed = 4krpm, specific load per pad = 2 MPa, μ= 0.2.

Figures 17 through 19 depict the predicted minimum film thickness, peak pressure, and pad maximum mechanical deformation for the example self-equalizing TPTB operating with φ= 0.01°($R_o\varphi$ = 11.25 μm) misalignment, versus sliding friction coefficient (μ)ranging from 0 to 0.3. Note that the friction forces acting at the contact points of the leveling plates restrict their tilting, i.e., they limit the desired action of the pad leveling system. The bearing operates at 4 krpm ($R_o\Omega$ =26.8 m/s) and under three loading conditions: a light specific load of 1.0 MPa per pad on the left side, a medium load of 2.0 MPa at the middle, and a heavy load of 3.0 MPa on the right side. Note predictions for an identical size regular TPTB (no self-leveling) are also included as a reference (shown with ▲).

In Figure 17, as the coefficient of friction increases, the minimum film thickness of the self-equalizing bearing reduces toward that of the regular bearing. For the heavily loaded operating condition with a zero friction coefficient, the self-equalizing bearing shows a minimum film thickness of 12.4 μm, and which is 54% larger than that of the regular bearing. As the friction coefficient increases to 0.3, the aligning ability of the pad leveling system lessens and the bearing minimum film thickness reduces to 10.7 μm.

In Figure 18, the pad leveling system proves effective to reduce the peak hydrodynamic pressure. The peak pressure on the regular TPTB is 19.3 MPa when operating under the heavy loading condition while using the self-equalizing bearing reduces the peak pressure roughly by half. Reducing the friction coefficient from 0.3 to 0 further reduces the peak pressure.

In Figure 19, the pad maximum mechanical deformations almost linearly increase with the pad specific load. Under the heavy applied load, pad mechanical deformations of the regular bearing are in the same order as the minimum film thickness. The pad maximum mechanical deformation of the self-equalizing bearing are roughly half of those of the regular bearing. Variations of the pad maximum mechanical deformation versus friction coefficient does not exceed 30% with respect to the predictions with zero friction.

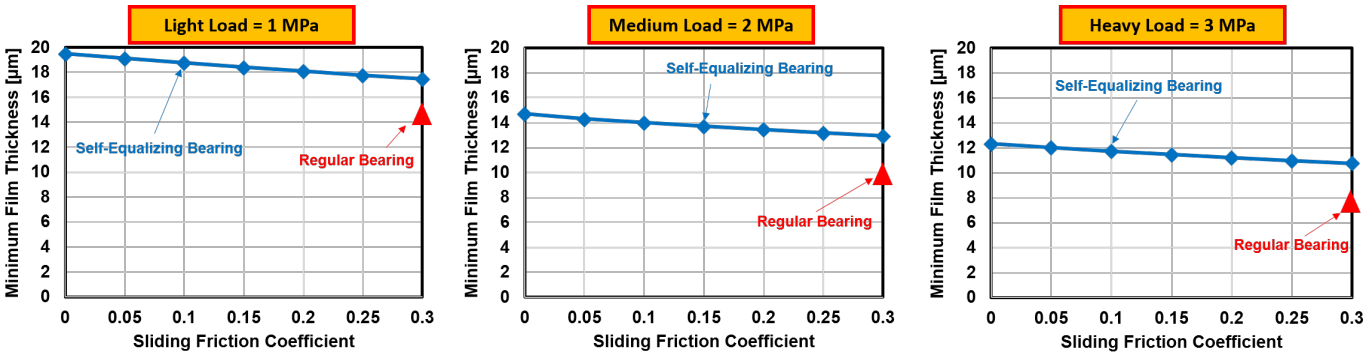

Figure 17: Predicted pad minimum fluid film thickness for self-equalizing TPTB operating under light to heavy applied loads vs sliding friction coefficient. Bearing operates with 0.01° thrust collar (static) misalignment. Applied load per pad = 1 MPa to 3 MPa and rotor speed = 4krpm.

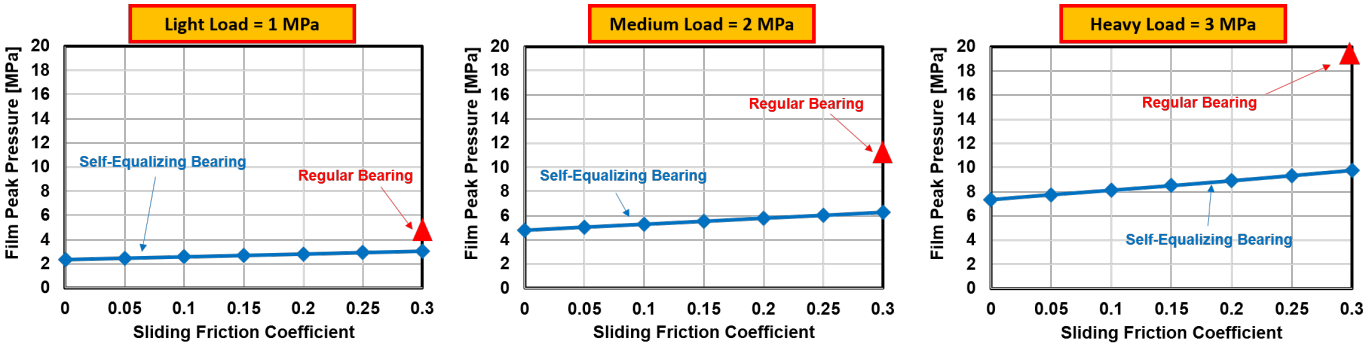

Figure 18: Predicted fluid film pressure on a pad for self-equalizing TPTB operating under light to heavy applied loads vs sliding friction coefficient. Bearing operates with 0.01° thrust collar (static) misalignment. Applied load per pad = 1 MPa to 3 MPa and rotor speed = 4krpm.

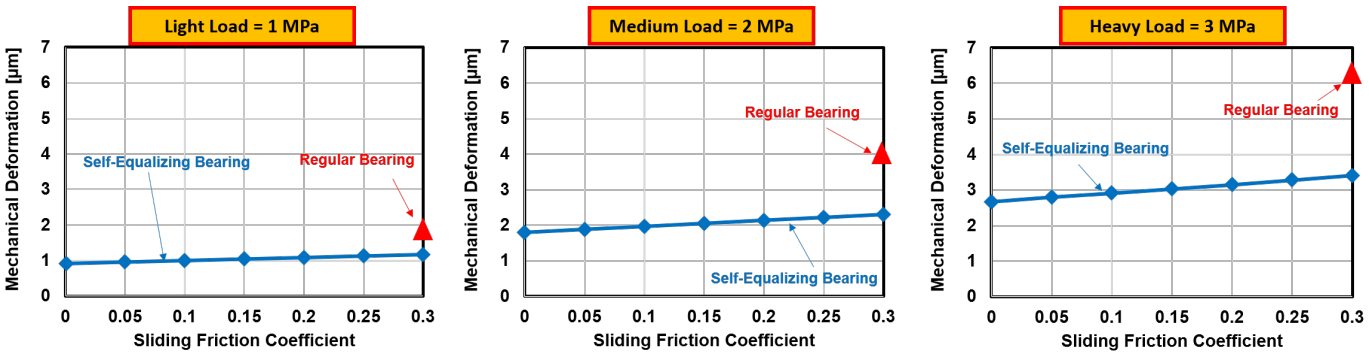

Figure 19: Predicted pad mechanical deformation for self-equalizing TPTB operating under light to heavy applied loads vs sliding friction coefficient. Bearing operates with 0.01° thrust collar (static) misalignment. Applied load per pad = 1 MPa to 3 MPa and rotor speed = 4krpm.

Figure 20 shows the predicted maximum Hertz contact pressure for the leveling plates of the example self-equalizing TPTB versus sliding friction coefficient. The bearing operates at 4 krpm rotor speed with φ= 0.01° thrust collar misalignment. As the pad specific load triples from 1.0 MPa to 3.0 MPa, the maximum contact pressure shows a roughly 80% increase, from less than 600 MPa to more than 900 MPa. Changes of the peak contact pressure versus friction coefficient are small though increasing.

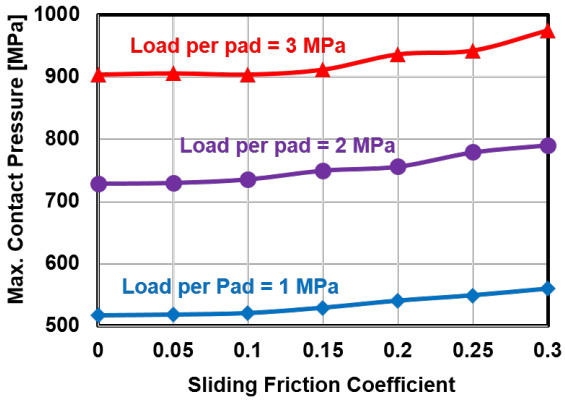

Figure 20: Maximum contact (Hertzian) pressure for the example bearing leveling plates vs sliding friction coefficient. Bearing operates with 0.01° thrust collar (static) misalignment. Applied load per pad = 1 MPa to 3 MPa and rotor speed = 4krpm.

CLOSURE

This report describes a model for the analysis of pad leveling mechanism coupled to a thrust bearing predictive tool [7, 8] to deliver load performance predictions for self-equaling tilting pad thrust bearings (TPTB). The analysis also includes the friction forces acting at the contact points of the leveling plates. Further a Hertz contact model determines the peak pressure over the contact area of the leveling plates as a function of the applied load on the bearing pads as well as the leveling plates geometry. Note the wear rate at the leveling plates contact area is proportional to the pressure and optimizing the design of the leveling plates to minimizing the peak contact pressure reduces the wear rate.

This report further presents load performance predictions delivered by XL_Thrustbearing® for an example self-equalizing TPTB operating under light to heavy loads, i.e., specific load per pad = 1 MPa to 3 MPa. The main findings are:

- For operation with thrust collar static misalignment, an ideal (without friction) self-equalizing TPTB operates with up to 50% larger minimum fluid film thickness and with a 60% lesser peak pressure compared to those detained in a regular TPTB.
- Friction forces acting at the contact points of the leveling plates show a significant effect on the performance of the pad leveling system as they reduce the film minimum film thickness and increase the pad peak pressure.
- Predictions from the Hertz contact analysis agree with those from a commercial finite element analysis tool and show a significantly large peak pressure at the contact points of the leveling plates.

Recommendation for Future Work

Future work could further the analysis to model leveling plates elastic deformations using a simplified analytical model or with a commercial computational finite element model. The magnitude of the friction coefficient over the contact area of the leveling plates is uncertain and changes from one contact point to another. Future work should account for the variable, often unexpected behavior of the friction coefficient and study its effect on the load performance of self-equalizing TPTB.

REFERENCES

[1] Glavatskih, S., 2002, "Laboratory Research Facility for Testing Hydrodynamic Thrust Bearings," *J. Eng. Tribol.,* **216**(2), pp. 105–116.

[2] He, M., Bryne, J. M., and Armentrout, R. W., 2018, "Fundamentals of Fluid Film Thrust Bearing Operation and Modeling," Asia Turbomachinery & Pump Symposium, Suntec, Singapore, 13-15 March; http://hdl.handle.net/1969.1/172449.

[3] Dadouche, A., DeCamillo, S. M., and Fillon, M., 2013, "Hydrodynamic Tilting-Pad Thrust Bearings," *Encyclopedia of Tribology*, pp. 1757–1765.

[4] Wodtke, M., Schubert, A., Fillon, M., Wasilczuk, M., and Pajaczkowski, P., 2014, "Large Hydrodynamic Thrust Bearing: Comparison of the Calculations and Measurements," *J. Eng. Tribol.,* **228**(9), pp. 974–983.

[5] Glavatskih, S., and Fillon, M. "TEHD Analysis of Thrust Bearings with PTFE-Faced Pads," *ASME Int. J. Tribol. Con.*, TRIB2004-64178, pp. 603–613.

[6] Heinrichson, N., and Santos, I., 2006, *"On the Design of Tilting-Pad Thrust Bearings,"* First Ed., Technical University of Denmark, Department of Mechanical Engineering, Institut for Mekanisk Teknologi, Lyngby, Denmark.

[7] San Andrés, L., and Koosha, R., 2017, "Thermo Hydrodynamic (THD) Computational Analysis for Tilting Pad Thrust Bearings (TPTBs)," TRC-B&C-05-17, Progress Report to the Turbomachinery Research Consortium, Texas A&M University, College Station, USA.

[8] San Andrés, L., and Koosha, R., 2018, "A Thermo-Elasto-Hydrodynamic (TEHD) Computational Analysis of Tilting Pad Thrust Bearings: Analytical and Fe Pad Structure Models," TRC-B&C-01-18, Progress Report to the Turbomachinery Research Consortium, Texas A&M University, College Station, USA., May 15-17.

[9] Heshmat, H., and Pinkus, O., 1987, "Misalignment in Thrust Bearings Including Thermal and Cavitation Effects," *J. Tribol.,* **109**(1), pp. 108–114.

[10] Glavatskih, S., and Fillon, M., 2001, "TEHD Analysis of Tilting-Pad Thrust Bearings-Comparison with Experimental Data," *Int. Tribol. Con., Japan Society of Tribologists*, pp. 1579–1584.

[11] Almqvist, T., Glavatskikh, S., and Larsson, R., 1999, "THD Analysis of Tilting Pad Thrust Bearings-Comparison Between Theory and Experiments," *J. Tribol.,* **122**(2), pp. 412–417.

[12] Souchet, D., 1991, "Comportement Thermohydrodynamique des Butées à Patins Oscillants en Régime Laminaire et Turbulent," PhD Dissertation, Universite de Poitiers, Poitiers, France.

[13] Pajaczkowski, P., Schubert, A., Wasilczuk, M., and Wodtke, M., 2014, "Simulation of Large Thrust-Bearing Performance at Transient States, Warm and Cold Start-up," *J. Eng. Tribol.,* **228**(1), pp. 96–103.

[14] Bavassano, F., Mantero, M., Traverso, R., Livermore-Hardy, R., and Blair, B., 2017, "A System Integration Approach for Heavy-Duty Gas Turbine Upgrades Using Improved Rotor Thrust Predictions and Application of Advanced Thrust Bearing Designs," ASME Turbo Expo 2017: Turbomachinery Technical Conference and Exposition, ASME Paper No. GT2017-63647.

[15] Wygant, K. D., Flack, R. D., and Barrett, L. E., 1999, "Influence of Pad Pivot Friction on Tilting-Pad Journal Bearing Measurements—Part I: Steady Operating Position," *J. Tribol. Trans.,* **42**(1), pp. 210–215.

[16] Cross, R., 2015, "Effects of Surface Roughness on Rolling Friction," *European J. Physics,* **36**(6), pp. 65029–65034.

[17] Myant, C., Spikes, H., and Stokes, J., 2010, "Influence of Load and Elastic Properties on the Rolling and Sliding Friction of Lubricated Compliant Contacts," *J. Tribol. Intern.,* **43**(2), pp. 55–63.

[18] Shigley, J. E., 2011, *Shigley's Mechanical Engineering Design,* Fourth Ed., pp. 161–166, Tata McGraw-Hill Education, New York, NY, USA.

[19] Popov, V. L., 2010, *Contact Mechanics and Friction: Physical Principles and Applications,* Second Ed., pp. 145-146, Springer, New York, NY, USA.

A. Appendix: Flowchart of the Pad Leveling Model

This model uses a numerical approach to find the location of a pad leveling mechanism upper plates as a function of the lower plates tilt angles. Figure 21 depicts a flow chart for the algorithm to find the location of a single upper plate. The flowchart repeats for all upper plates in the pad leveling system.

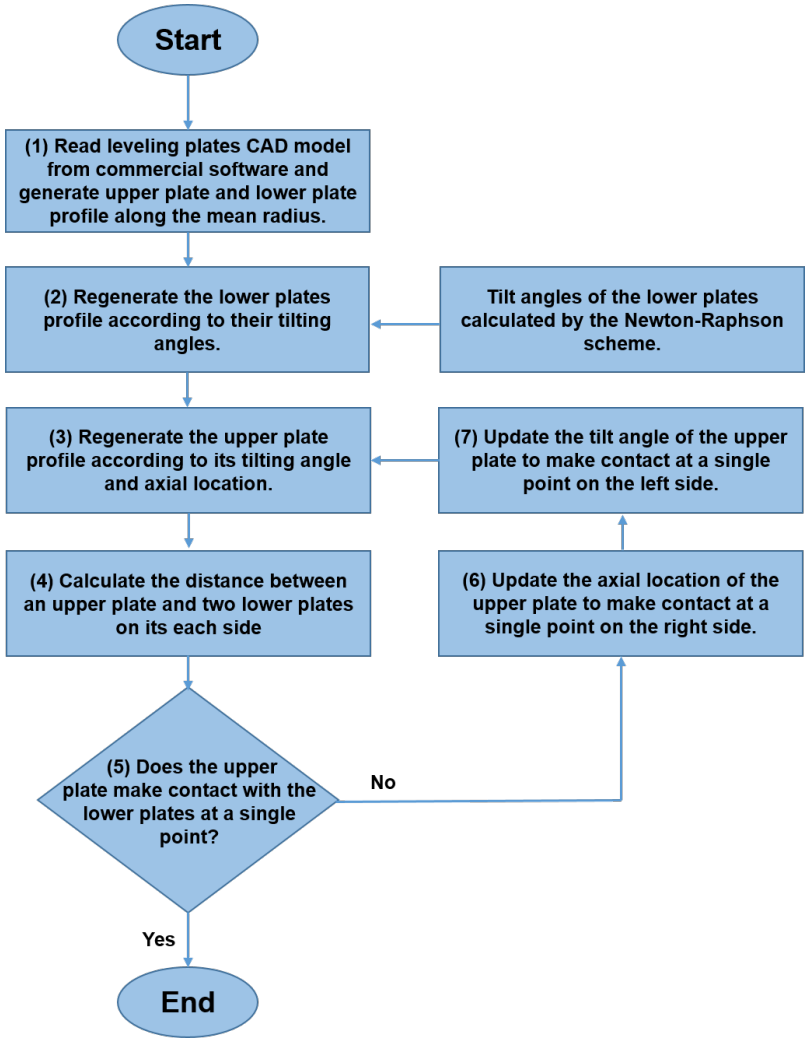

Figure 21: Flowchart of algorithm used to find the location of an upper plate as a function of the power plates tilt angles.

The following explains the algorithm step by step.

- Step (1) generates a 2D profile of both the upper plates and the lower plates using their CAD model from the a commercial solid modeling software.
- Step (2) regenerates the lower plates profile according to their tilt angles. Recall that a Newton-Raphson approach determines a tilt angle for the lower leveling plates based on the moments acting on them.
- Step (3) regenerates the upper plate profile based on its axial location and tilt angle.
- Step (4) calculates the axial distance between the upper plates and the lower plates on each side. The final goal is for the upper plate to make contact with the lower plates at a single point. Hence the distance between the upper plate and the lower plate is zero at a single location.
- Step (5) checks to see if the upper plates is making a single point contact with the lower plates on its sides. If yes, the program ends.
- Step (6) relocates the upper plate axially to make a single point contact with the lower plate on its right side.
- Step (7) tilts the upper plate to make a single point contact with lower plates on its left side. Note the single point contact condition on the right side made in Step (6) may no longer hold as the upper plate tilts.
- Program repeats from Step 3.